# A realistic deformable prostate phantom for multimodal imaging and needle-insertion procedures

Nikolai Hungr, Jean-Alexandre Long, Vincent Beix, Jocelyne Troccaz

# A realistic deformable prostate phantom for multi-modal imaging and needle-insertion procedures

Nikolai Hungr [a)]
*UJF-Grenoble 1 / CNRS / TIMC-IMAG UMR 5525 (Equipe GMCAO), Grenoble, F-38041,France*

Jean-Alexandre Long
*Clinique Universiatire de Chirurgie urologique et Transplantation rénale, CHU Grenoble, 38043 Grenoble Cedex 9*

Vincent Beix
*UJF-Grenoble 1 / CNRS / TIMC-IMAG UMR 5525 (Equipe GMCAO), Grenoble, F-38041, France*

Jocelyne Troccaz
*UJF-Grenoble 1 / CNRS / TIMC-IMAG UMR 5525 (Equipe GMCAO), Grenoble, F-38041,France*

**Purpose:** Phantoms are a vital step for the preliminary validation of new image-guided procedures. In this paper, we present a deformable prostate phantom for use with multi-modal imaging (end-fire or side-fire ultrasound, CT and MRI) and more specifically for trans-perineal or trans-rectal needle-insertion procedures. It is made of soft polyvinyl chloride (PVC) plastic and includes a prostate, a perineum, a rectum, a soft periprostatic surrounding and embedded targets for image registration and needle-targeting. Its main particularity is its realistic deformability upon manipulation.

**Methods:** After a detailed manufacturing description, the imaging and mechanical characteristics of the phantom are described and evaluated. First, the speed of sound and stress-strain relationship of the PVC material used in the phantom are described, followed by an analysis of its storage, imaging, needle insertion force and deformability characteristics.

**Results:** The average speed of sound in the phantom was measured to be 1380±20 m/s, while the stress-strain relationship was found to be viscoelastic and in the range of typical prostatic tissues. The mechanical and imaging characteristics of the phantom were found to remain stable at cooler storage temperatures. The phantom had clearly distinguishable morphology in all three imaging modalities, with embedded targets that could be precisely segmented, resulting in an average US-CT rigid registration error of 0.66 mm. The mobility of the phantom prostate upon needle insertion, was between 2 and 4 mm, with rotations between 0° and 4°, about the US probe head.

**Conclusion:** The phantom's characteristics compare favorably with in vitro and in vivo measurements found in the literature. We believe that this realistic phantom could be of use to researchers studying new needle-based prostate diagnosis and therapy techniques.

Key words: deformable phantom, prostate, needle insertion, multi-modal imaging, PVC

## I. INTRODUCTION

Prostate cancer is the third most deadly cancer in men in western developed countries, with 33 720 and 70 821 deaths estimated in 2011 in the US[1] and in 2008 in Europe[2], respectively. Indeed, the importance of this disease

on public health is such that it has attracted an abundance of research in improved diagnostics and therapy over the last decade. Percutaneous trans-perineal and trans-rectal interventions for the diagnosis and treatment of prostate cancer have seen particular attention due to their minimally-invasive approaches. In recent years, important developments have been made in computer and robot-assisted image-guided needle insertion technology. The most common imaging modality used for such prostate techniques is ultrasound (US), due to its harmless, inexpensive and easily accessible nature. CT and MRI, however, have also seen a lot of research attention because of their complementary imaging characteristics.

For any new developments in the field, anthropomorphic phantom-testing is a pre-requisite before doing animal or human testing. Prostate phantoms are artificial models of the prostatic environment that emulate soft tissue mechanical and imaging characteristics. A wide variety of such phantoms have been developed, typically to meet certain simplified project-specific needs. Phantom applications have included: the evaluation of needle insertion accuracy, the validation of biomechanical models, testing of image processing algorithms, preliminary studies on new treatment methods, and surgeon training, amongst others.

In this paper, we describe a deformable prostate phantom that we developed and that we believe could be of potential use to the research community. We begin the paper with a description of the context and reasoning for the development of our phantom followed by a review of existing prostate phantoms, their characteristics and particularities. We then discuss the various phantom materials cited in the literature and what material we chose for our phantom. We then describe our phantom in detail, including its ingredients and construction recipe. In the second half of the paper, we describe the phantom's mechanical and imaging characteristics, concluding with a discussion of its novelty, usefulness and limitations.

### I.A. Context

In our laboratory, we have developed a robotic brachytherapy needle insertion system which uses a robotic needle insertion device coupled to a 3D US registration software to track prostate motion intra-operatively. The prototype of the robotic device and the US registration software have both been described in previous publications.[3-5] The primary goal of our system is to improve accuracy and efficiency of seed deposition in prostate brachytherapy by taking into account tissue mobility during needle insertion.

The first step for bringing this project to clinical trials was to run a phantom study to determine the system's accuracy, efficiency, ergonomics and reliability. The novelty of our system is its ability to track prostate motion, so it was vital that our phantom be able to simulate prostate motions during needle insertion. For this purpose, we were interested in developing a prostate phantom that had the following anatomical morphology:

- prostate: to validate our registration technique;
- general periprostatic tissue: to hold the prostate in place while allowing prostate mobility;
- skin of the perineum: to simulate realistic needle-tissue interactions during insertion;
- rectum: to allow for realistic insertion of either an end-fire or a side-fire US probe;

- urethra: (optional) to make the US images more realistic for both dose planning and image registration.

The phantom study that we carried out involved the insertion of a number of inert brachytherapy seeds in the phantom using US guidance, based on a mock seed plan conceived beforehand. Accuracy was measured by comparing the deposited seeds to the dose plan using post-implant CT imaging. Beads placed within the phantom during construction were used either as targets or for US-CT image registration.

## I.B. Prior art

A large number of prostate phantoms have been described in the literature over the last decade. Everything from very simple uniform blocks, to more complex and realistic multi-component phantoms, to commercialized tissue-equivalent phantoms. Their main features are 1) to reproduce the anatomy of the prostate environment, 2) to emulate the soft-tissue feel either for applying surface pressure or for needle insertion and 3) to emulate the imaging characteristics of the prostate, whether it be X-ray, MRI or US based. The variety of phantoms designed nearly equals the variety of prostate applications being researched.

The simplest phantoms are uniform single-component phantoms. Their simplicity has been used for preliminary studies in a very controlled environment, such as the initial validation of new needle insertion instruments[6-8] as well as the validation of image processing techniques such as brachytherapy seed segmentation.[9] Uniform phantoms impregnated with a matrix of visible fiducials have also been built for experimental validation of biomechanical models.[10-12]

For prostate-based percutaneous procedures, multi-component phantoms are more useful as they introduce more realistic anatomical conditions, both mechanically and for imaging. Some examples of such phantoms can be seen in the work by Bax *et al.*[13] and Long *et al.* [14], both of which include a prostate suspended in background material. A number of studies have also used an industrial prostate phantom commercialized by CIRS (Computerized Imaging Reference Systems, Inc).[15,16] This phantom consists of prostate and seminal vesicles embedded in surrounding tissue and has a perineal surface, along with a rectum and urethra. None of these phantoms were designed to simulate prostate motion.

Few publications exist that describe the use of a phantom specifically for prostate motion evaluation. The earliest “mobile prostate phantom” that we found in the literature was described by McGahan *et al*,[17] and was used to determine errors caused by external probe pressure during radiotherapy. The hard prostate, made of clay, makes this phantom, however, inappropriate for needle insertion. Only two other mobile phantoms were found that were designed specifically for needle insertion. Both use a harder prostate encapsulated in softer surrounding polyvinyl chloride (PVC) material. In Dehghan *et al.*[18] the phantom has a rectum as well as a stiffer inclusion linking the prostate to the base of the phantom in an attempt to reproduce the prostate’s rotation about the pubic bone. Needle insertion into the phantom resulted in axial prostate motions of <4 mm. The phantom described by Sherman *et al.*[19] has the added characteristic of Including a perineal surface, simulated with a 2cm layer of stiffer material. The phantom was used in a vertical orientation, with two orthogonal US probes for visualization.

Vitamin E capsules were embedded in the phantom to provide specific targets for motion tracking. Target motions up to 11mm were reported during needle insertion.

These last two mobile phantoms were the closest to our design objectives and we used them as inspiration for our own design. Our initial building block was therefore the use of a harder prostate embedded in a softer surrounding. Our main goal was then to improve the anatomical realism, adapt the phantom for transrectal ultrasound applications and ensure its multi-modality to generalize its usability. The resulting phantom was found to have very satisfying mechanical and imaging characteristics that we report in this paper in detail.

### I.C. Phantom materials

To satisfy our design constraints, we had to choose an appropriate material for our phantom.

Some of the most common base materials used in phantom construction are agarose, gelatin, polyvinyl alcohol (PVA-C), polyvinyl chloride (PVC), silicone and the proprietary commercialized material Zerdine (CIRS). Their mechanical and imaging characteristics are described by various sources, comparing them to real tissue. Table I summarizes the various properties of these materials found in the literature. A detailed description of each of these materials can be consulted as electronic supplemental material.

We experimented with all of the above materials, settling on the following conclusions: agarose and gelatin are too fragile for the type of motions we require, especially when low concentrations are used for the surrounding periprostatic material; the CIRS phantoms do not have evident deformation during needle insertion and are expensive, making them impractical for tests requiring multiple phantoms; PVA-C has a very complex and lengthy preparation procedure which makes it challenging for multi-component structures; silicone has inappropriate acoustic properties. Our choice was therefore PVC, which provides the best compromise between mechanical and imaging characteristics. It has a sufficiently large range of elastic modulus all the while remaining resistant to rough handling (needle puncture, probe pressure, etc), and is inexpensive and simple to manufacture.

## II. MATERIALS AND METHODS

### II.A. Phantom Description

The phantom that we developed is shown in Figure 1. It consist of four distinct regions made of PVC mixtures of various elasticities. Soft PVC can be bought from companies that specialize in fishing lure construction, such as M-F Manufacturing Co., Inc. (Ft. Worth, Texas),[18,26,38] or, in our case, Bricoleurre (Mont Saint Aignan, France). The PVC used in our phantoms consists of a mixture of PVC polymer solution and the softener diethyl hexyl adipate. Our provider sells PVC in a number of different pre-mixed polymer-softener mixtures, the stiffest being a “super rigid” mixture, whose exact ratio of polymer-softener is proprietary and could not be obtained. Based on this super rigid mixture, various softer mixtures can be obtained by adding an appropriate amount of

softener solution. The PVC mixtures that we used during our experiments and in our phantom are listed in Table II.

As described in the introduction, the anatomy that we wished to simulate with our phantom includes: 1) the perineum, 2) the rectum, 3) the prostate, 4) the surrounding periprostatic tissue, and 5) an optional urethra for imaging purposes. The perineum acts as the first "tougher" skin barrier through which the needle must traverse. It also provides a structural frame to maintain the phantom's form. The rectum accepts an end-fire US probe and is strong enough to resist rough handling during probe placement. The prostate has a colored capsule that makes it visible both to the human eye as well as in ultrasound images. The prostate is hard enough to be mobile but soft enough to be deformable upon needle insertion, as will be described in Section III. The periprostatic tissue suspends the prostate in place within the phantom. It is soft enough to allow for sufficient prostatic mobility during ultrasound probe handling and needle insertion.

### II.B. Phantom Construction

The construction of the phantom is illustrated in Figure 2. It requires simple equipment: a laboratory hot plate, a 1.5 L pot, a 300 mL beaker and an optional vacuum chamber. Material costs for a single phantom are on the order of $20 to $25 US. A single phantom takes about 5 hours to make (3 hours for the frame, 1 hour for the prostate and 1 hour for the surrounding material and overall assembly), and requires 12 hours of curing time after final assembly. Multiple phantoms can be made in parallel if the equipment is available. Two moulds were constructed, one for the frame and rectum and one for the prostate. The former (Figure 2(a)) was made of aluminum and was a negative of the frame and rectum seen in Figure 1. The prostate mould was an approximation of a prostate geometry imprinted into fast-drying silicone paste.

To make the 9 x 10 x 15 cm frame, a standard mixture (see Table II) is heated in the pot at a hot plate temperature of 450˚C for 30 minutes, until polymerized. The solution is poured into the aluminum mould and cooled at room temperature. An appropriate molding technique must be used to ensure that no air remains trapped in the mould: in addition to appropriate mould orientation with respect to gravity, the mould can be placed in a vacuum chamber for 1 to 2 minutes immediately after pouring of the PVC. It is helpful to preheat the mould on a heating element to prevent the PVC from curing too quickly around the thin walls thus trapping the escaping air bubbles. This procedure, including cooling, takes about three hours.

For the prostate, the same standard PVC mixture is heated in a 300 mL beaker at 450˚C for 20 minutes (Figure 2(b)). As soon as full polymerization has occurred, the beaker is ideally placed into the vacuum chamber for 1 to 2 minutes. The pressure change induces a boiling effect. Upon pressure release, all air bubbles disappear from the solution and it can be poured carefully into the mould (Figure 2(c)). At this stage, it is possible to embed reference targets inside the prostate. This is done by pouring the PVC into the mould in layers, briefly letting each layer to cool at its surface just enough to place the targets without them sinking (about 3-4 minutes), and then covering them with the next layer of PVC (Figure 2(d)). The beaker can be kept on very low heat (hot plate temperature of 100˚C) during this procedure to keep it from curing.

Two types of targets were tested: glass and polymer clay beads. 1mm diameter glass beads can be obtained from laboratory equipment merchants and have good US and CT imaging characteristics. Polymer clay targets can be shaped into 1mm diameter beads and baked in an oven at 130°C for 20 minutes. Similar to soft PVC, polymer clay is a PVC-based material sold for hobbies and crafts. It has good US, CT and MRI imaging characteristics. Its advantage over glass beads is that it does not cast a white shadow in US images, keeping the image clear. Glass beads are, however, more easily and precisely distinguishable in the image.

The prostate mould is made with a 2 to 3 cm tail on its base (Figure 2(e)). This allows it to be held with ease during coating of the prostate capsule material. The capsule material is made by heating standard PVC in a beaker and, once polymerized, mixing in a scattering agent. In our phantoms, we used 0.2 grams of the biological staining agent Toluidine Blue for 200 mL of PVC material. This made the prostate contour not only echogenic in ultrasound, but also made it blue and visible within the surrounding transparent PVC. The prostate is dipped once or twice into the stained PVC solution, depending on the desired capsule thickness. Once cooled, the prostate tail can be cut off and the exposed base can be re-dipped into the stained PVC to complete the capsule (Figure 2(f)). The prostate and capsule take approximately one and a half hours to make.

The suspension of the prostate within the frame and surrounding material is done by first pouring an initial layer of super soft PVC periprostatic material (heated at 450˚C for 20 minutes) to the appropriate height, letting it cure enough to place the prostate in position (Figure 2(g)) and then filling up the rest of the frame. If no bubbles are desired, each layer can be placed in the vacuum chamber for 1 to 2 minutes as described above. Additionally, a small amount of scattering agent can be mixed with the periprostatic material to increase its echogenicity for more realistic ultrasound images. Curing of this very soft PVC at this stage takes much longer and ideally should be left overnight (Figure 2(h)).

An optional urethra can be included in the prostate. For this, a thin tube is inserted into the prostate mould before pouring. This makes a hole through the prostate which can then be filled with a mixture of standard PVC and scattering agent before creating the prostate capsule. Another variation to the phantom is to place targets outside of the prostate, into the periprostatic material. This is done by layering, in the same way as for the prostate.

PVC is amenable to layering. Although layers of different elasticities can be separated by hand, they bond together amply for needle-insertion purposes. Bonding is improved when the second layer is poured before complete cooling of the first layer, as it allows the polymer chains between layers to blend together. An important precaution to note during the preparation of soft PVC is not to overheat the PVC, as it burns very quickly (overheating is evident as the solution turns dark yellow). Stirring is therefore very important. Magnetic stirrers were not found to be ideal, as the PVC tends to solidify prematurely around it during heating. A more efficient technique is to stir regularly by hand, and then use the vacuum chamber to eliminate bubbles.

## III. PHANTOM CHARACTERISTICS

The phantom has a number of distinct characteristics, both in its mechanical behavior and its imaging compatibility. Its primary feature is the mobility of the prostate both when manipulating an ultrasound probe in the rectum and when inserting a needle. In addition, the different anatomical regions in the phantom are clearly distinguishable in US, CT and MRI. These properties will be discussed in further detail in the sections that follow.

## III.A. Speed of sound

In order to acquire accurate ultrasound images of the phantom, it was necessary to know the speed of sound in the PVC material used. The speed of sound was measured by fixing an US transmitter at a set distance from the floor of a water-filled basin. The speed of sound of the water was calculated based on its temperature and the distance between the transducer and the basin as measured in the image. A sample of the PVC material was then placed between the transducer and basin floor and the distance was measured again. A simple proportion calculation gave us then a value for the speed of sound in the PVC:

$$c_{PVC} = c_{water} \frac{d_{water}}{d_{PVC}}$$

The experiment was repeated over the range of PVC mixtures used in the phantom and the results are shown in Table II. The first three measurements were carried out by medical ultrasound transducer manufacturer, Vermon, in their research facility, using material specifically designed for this purpose (notably a 3.5 MHz emitting transducer coupled to a receiving transducer on the floor of the water basin) . Due to technical reasons, Vermon was unable to do the fourth measurement so it was done in our laboratory using an 8MHz linear array US transmitter connected to an Ultrasonix Sonix TOUCH ultrasound machine.

The values that we measured were compared to results published in the literature. Spirou *et al.*[26] report a speed of sound of 1400±20 m/s. It is unclear, however, how their PVC material compares to the various mixtures that we tested. Madsen *et al.*[27] report a similar value of 1395 m/s, but with no details on how the values were measured and what type of PVC mixture was used. Nevertheless, both reported values fall within the range of our measurements. With these results, we were able to determine the speed of sound with which to acquire US images of the phantom with minimal distortion error. To do so, we took the speed of sound at the two extreme depths of the prostate: one at the point closest to the probe head, and one at the point farthest from the probe head, as shown in Figure 3. The two speeds were calculated based on the depth-weighted average of PVC mixtures that the sound wave must travel through. The final speed of sound used for the phantom was taken as the average of these two extremes: 1380±20 m/s. The variability in speed of sound due to the varying depths of PVC mixtures would cause an error of ±1.5% of the distance from the probe head. For the shallowest areas (~20 mm from the probe head), this would amount to about 0.3 mm, while for the deepest areas of the prostate (~60 mm), the error could be up to 0.9 mm. We consider this variability reasonable, as it is less than the variability due to tissue differences reported in vivo.[39,40]

We verified the speed of sound by manually segmenting the prostate in a 3D US image and comparing it to the true volume of the prostate. The US volume was reconstructed at 1380 m/s with an Ultrasonix 4DEC9-5 end-fire probe connected to an Ultrasonix RP ultrasound machine, giving a 299 x 299 x 299 image with a voxel dimension of 0.33 mm. The true volume was determined during construction of the phantom by measuring the volume of water displaced when submerging the prostate. The segmented volume of the prostate was 47.2 $cm^3$ compared to the true measured volume of 47.0 $cm^3$. The proximity of the two results lead us to believe that the chosen speed of sound was suitable.

### III.B. Stress-strain relationship

To compare the PVC material's elastic properties to those of prostatic soft tissue, the stress-strain relationship of the various mixtures was studied. The compression stress-strain relationship was measured using a Gabo Eplexor (Ahlden, Germany) mechanical characterization machine, as shown in Figure 4. Five 16 mm diameter cylindrical samples of the five different PVC mixtures described in Table II were prepared and allowed to settle overnight. A 25 N force transducer was used to measure a 35% compression-decompression cycle at 0.5 mm/s for each sample. The same measurements were also made on 3 sets of identical samples prepared 11 days before, in order to study the stability of the samples over time. These stability results will be described in the following section.

The resulting stress-strain curves are shown in Figure 5. For all the samples, the curve shows viscoelastic behavior, with an increase in elastic modulus with increasing strain and a hysteretic effect between compression and decompression cycles (caused by the relaxation of the material during deceleration of the compressor). A quadratic polynomial fit to the first set of fresh samples is shown in Figure 5. To get an idea of the difference in elasticity of the five PVC mixtures used, we can make a linear approximation of the first part of the stress-strain curves (up to 20% compression strain). The results are shown in Table II and correspond with published results for both PVC and in vitro prostate tissue.[41-43]

### III.C. Phantom storage characteristics

The ability to store a phantom without a change in its properties over time, is an important aspect in phantom design. Extensive testing of systems often requires phantoms to be made in batches in advance, before actually beginning the experiments. It is very important, therefore, that the phantom properties remain consistent throughout the testing period. We carried out two experiments to verify the response of our PVC phantom over time with respect to its two primary properties described above: speed of sound and stress-strain. The main goal was to determine the best storage conditions for our phantom.

The first experiment involved measuring the compression stress-strain relationship for various PVC samples stored 1) at room temperature (between 23˚C and 25˚C), 2) in the fridge (4.5˚C) and 3) in the freezer (-21˚C). The resulting stress-strain relationships can be seen in the electronic supplemental material. The results show that the stress-strain relationship follows a steeper curve with increasing storage temperature. In other words, the higher

the storage temperature, the stiffer the PVC becomes over time. The freezer would therefore seem to be the best storage environment for PVC, in order to conserve its mechanical elasticity.

In the second experiment, we constructed three small sample phantoms with an echogenic inclusion, similar in property to the true phantom. These samples were once again stored at room temperature, in the fridge and in the freezer, and observed visually and with ultrasound, over a period of 26 days. The sample stored in the freezer showed noticeably less changes in visual aspect, compared to the other samples. To analyze the 3D US images of the samples, the volume of the echogenic inclusion visible in the images was measured. The results can be seen in Figure 6 and show an increase in inclusion volume over time, with the freezer samples being less affected than the room temperature samples. This volume change can be attributed to an increase in speed of sound, which is a reasonable assumption, given the increase in stiffness of PVC over time, as described in the previous paragraph (see also measured speeds for mixtures of various stiffnesses in Table II).

Based on these results and observations, it was evident that it was best to store the phantoms in the freezer, at low temperatures, to minimize changes in mechanical and imaging properties. Please note that interested readers can refer to the detailed description of the experiments and their results in the electronic supplemental material.

### III.D. Imaging characteristics

Phantoms that are visible in multiple imaging modalities are valuable, because they do not restrict their use to just a single type of image-guided procedure. Complementary information can also be extracted from the different imaging modalities and combined to provide more a complete analysis of the phantom tests. For example, the distribution of brachytherapy seeds inserted under US guidance can be analyzed in a CT scan volume. An important aspect of our phantom design was, therefore, its multi-modality.

We have tested our phantom in the three primary volumetric imaging modalities: ultrasound, CT and MRI. US images of the phantom can be seen in Figure 7. The prostate capsule, which is blue to the naked eye, stands out as the white outer boundary of the prostate. The figure shows two types of embedded targets: the polymer clay targets cast a small black shadow and their outline can be clearly seen; the glass targets cast slight white shadows that that allow for very easy and accurate segmentation. A 3D prostate registration algorithm developed in our laboratory for biopsy targeting and brachytherapy guidance[3,4] was tested and works flawlessly.

The main disadvantage of this phantom, like with the majority of synthetic phantoms, is that needle insertions leave permanent traces in the US images. In our experience, this limited us to about 15 to 20 insertions per phantom, before the image became too degraded for effective use. At this point, the registration algorithm started showing inaccuracies in certain noisier areas of the volumes.

Figure 8 shows a CT and an MR image of the phantom. In the CT image, the PVC mixtures used in the phantom are clearly distinguishable because of their different densities. The Hounsfield Units for the various PVC mixtures were determined and are listed in Table II. In the MR image, the phantom is equally visible, with the prostate, prostate capsule and urethra clearly distinguishable. The polymer clay and the glass targets are visible in both modalities and are easily segmented.

To check the segmentation accuracy of the targets in the images, we compared US and CT images of 8 phantoms embedded with 8 to 12 glass targets each. The targets were segmented manually at high zoom in each US and CT image. The clouds of segmented US points were then rigidly registered to the corresponding CT points using Arun least squares fitting.[44] The average registration error for all 8 phantoms was 0.66 mm. This error is very reasonable, as it includes the segmentation errors from both modalities. A similar test including MR images was not done because of availability constraints for the high-demand clinical MR machines at our disposal.

### III.E. Needle insertion force

To study the mechanical behavior of our phantom specifically during needle insertion, we measured the axial force required to push a 19 gauge diamond-tip Mick Ripple-Hub needle (Mick Radio-Nuclear Instruments, Inc.) into the prostate. This was done by mounting a Flexiforce A201 force sensor (Tekscan) onto the brachytherapy needle insertion robot described in Hungr *et al.*[5] and calibrating it by applying known forces on the needle tip. A plot of the insertion force measured by the force sensor during insertion through the perineum and into the prostate of our phantom is seen in Figure 9. The different regions of the phantom through which the needle traverses can be distinguished and are labeled in the figure. A first maximum is reached, at 1.8 N, when traversing the perineum. The force then decreases through the periprostatic region, until it reaches the prostate. It then increases as it travels through the prostate, until the needle is stopped. At this point, we see a decrease in the force, as the material relaxes around the needle. This multistep behavior is comparable to the in vitro liver puncture curve reported by Maurin *et al.*,[45] the dog prostate tests described by Kataoka *et al.*,[46] as well as the in vivo force measurements done by Podder *et al.*[38] during live brachytherapy.

Although the axial force curve has a characteristic shape for prostate needle puncture, our partner urologists have mentioned that the increasing friction felt the deeper the needle is pushed, is not realistic. In a real patient, blood lubricates the shaft of the needle, making the needle tip cutting force the primary force felt by the clinician, allowing them to feel the needle's progress through different tissues. The phantom, on the other hand, is not lubricated, and as the cutting force is relatively low compared to the friction between the PVC and the needle shaft, it is more difficult for the clinician to "read" the tissues with the needle.

### III.F. Prostate motion

Prostate motion is the primary behavioral aspect that we wished to reproduce in our phantom. We wished to use it to evaluate our prostate tracking system for robotic brachytherapy. In the literature, it has been shown that prostate motion is important during needle insertion.[47-49] It has been suggested that in vivo motion of the prostate is constrained by the ligament bundles holding the prostate to the pubic arch above, resulting in translation and rotation of the prostate.

To quantify the amount of motion caused by needle insertions in our phantom, we looked at the deformation fields calculated by our registration algorithm for five different insertion locations in the prostate, as shown in

Figure 10. The deformation fields were obtained by registering a reference 3D US image taken before insertion to a second image taken after needle insertion. Insertions were done using a robotic insertion device, using an 18 gauge Mick Ripple-Hub needle, with an insertion speed of 5 mm/s. After each insertion, an image volume was acquired to which the reference image taken before insertion was registered. A grid of 512 points evenly distributed throughout the prostate, were taken from the resulting 3D deformation field and used to analyze the prostate motion. The center of mass of the points was used to quantify the amount of translation experienced by the prostate. The rotation of the prostate was extracted from the transformation matrix determined by rigidly registering the grid points from the before and after US volumes using Arun least squares fitting.[44] The results are shown in Table III for the five insertions done on a single phantom.

We found, as can be expected, that the prostate motion depended on the direction and location of insertion of the needle, and was generally constrained to motion about the fixed US probe head inside the rectum. A needle inserted straight into the center of the prostate, resulted in translational motion along the needle axis direction. An angled approach from the side of the prostate, resulted in a translation of the prostate along the needle axis direction coupled with a rotation about the probe head. The translation and the coronal-plane rotation of the phantom prostate was realistic, compared to the motions described in the literature. Rotation in the sagittal direction, was, however, different, as rotation tended to be downward towards the rectum, rather than upward towards the pubic arch as suggested in the literature. But, as also mentioned in the literature, the sagittal-plane rotation is not as important as other motions, and tends to be unpredictable in any case.[47] The measured translations and rotations correspond to published results measured in vivo: on the order of 3 to 10 mm of translation[48] and between 0 and about 10 degrees of rotation.[49]

### III.G. Precautions

There are some precautions to be taken when using this phantom. Although the construction technique is quite simple, it does require some caution in order to produce repeatable phantoms. The primary difficulty lies in the reduction of air bubbles. If a vacuum chamber is not used during construction, bubbles can become difficult to avoid. It is also important to heat the PVC material in the same way for each phantom, to ensure visible similarity, although differences in the heating procedure did not affect the imaging characteristics. Another precaution lies in the toxicity of the fumes emitted by the heated PVC. Although authorized for general public use, the fumes are very unpleasant to inhale, and the PVC should be handled under a fume hood during construction. The speed of sound, lower than the 1540 m/s used in standard US machines, may also be a difficulty for those unable to modify the sound speed used in their image reconstructions. Such a situation, however, is not wholly unreasonable, as the variations in speed of sound in the real prostatic environment are important.[39,40] Although much better than water-based materials, the storage of PVC must nevertheless be handled with caution, and the phantoms should ideally be stored at cool temperatures. Finally, the material is also able to react with other types of PVCs, so ultrasound probes should always be used with a protection cover to prevent possible damage.

## IV. CONCLUSION

The prostate phantom described in this article has the characteristics of being realistically mobile upon needle insertion, as well as being visible to the naked eye and in US, CT and MR images. We have used it for the preliminary validation of a new robotic brachytherapy system that includes 3D US-US registration. We believe that this phantom could be useful to other research teams working on similar prostate intervention technologies. Phantom validation is a necessary first step in most, if not all, new diagnostic or therapeutic techniques. A multitude of phantoms have, therefore, been described in the literature, but very few have the realistic mechanical and multimodal imaging characteristics presented above, and certainly none have been described to sufficient detail to allow for reproduction by interested readers.

The phantom is relatively fast to construct, does not require special tools for fabrication, and is inexpensive in material costs. For ultrasound applications, although only an end-fire probe version was described here, the rectum can easily be adapted to accept a side-fire probe, as shown in Figure 11. The morphology of the phantom allows for both trans-rectal and trans-perineal needle approaches. The imaging characteristics of the phantom also make it useful for testing the accuracy of both feature-based and intensity-based deformable registration techniques.

## ACKNOWLEDGMENTS

The authors would like to thank Dr. Ivan Bricault and the staff of the radiology department of the Grenoble University Hospital (CHU Grenoble) for their unfailing availability and willingness to scan our countless phantoms.

[a)]Author to whom correspondence should be addressed. Electronic mail: Nikolai.Hungr@imag.fr

[1]Cancer Society. Cancer Facts and Figures 2011 [Online]. Available: http://www.cancer.org (2012, January 13).

[2]J. Ferlay, D.M. Parkin, E. Steliarova-Foucher. “Estimates of cancer incidence and mortality in Europe in 2008,” Eur. J. Cancer, 46(4),765-81 (2010).

[3]M. Baumann, P. Mozer, V. Daanen, J. Troccaz, “Prostate biopsy assistance system with gland deformation estimation for enhanced precision,” *Med. Image Comput. Comput. Assist. Interv. – MICCAI*, 12 (Pt 1), 67-74 (2009).

[4]M. Baumann, P. Mozer, V. Daanen, J. Troccaz, “Prostate biopsy tracking with deformation estimation,” Med. Image Anal. In press (2011)

[5]N. Hungr, J. Troccaz, N. Zemiti, N. Tripodi, “Design of an Ultrasound-Guided Robotic Brachytherapy Needle-Insertion System,” *Annual International Conference of the IEEE Engineering in Medicine and Biology Society-EMBC*, (Minneapolis, 2009), pp. 250-253.

[6]R. Lefrançois and R. S. Sloboda, “A medical needle drive for the study of interstitial implant mechanics,” Med. Eng. Phys. 25(3), 255-258 (2003).

[7]Y. Yu, T. Podder, Y. Zhang, W.S. Ng, V. Misic, J. Sherman, L. Fu, D. Fuller, E. Messing, D. Rubens, J. Strang and R. Brasacchio, "Robot-Assisted Prostate Brachytherapy," Med. Image Comput. Comput. Assist. Interv. 9(Pt 1), 41-49, (2006).

[8]M. P. Ottensmeyer and J. K. Salisbury, "In Vivo Data Acquisition Instrument for Solid Organ Mechanical Property Measurement." Lecture Notes in Computer Science, 2208, 975-982 (2001).

[9]M. De Brabandere, C. Kirisits, R. Peeters, K. Haustermans and F. Van den Heuvel, "Accuracy of seed reconstruction in prostate postplanning studied with a CT- and MRI-compatible phantom," Radiother. Oncol. 79(2), 190-197 (2006).

[10]A. E. Kerdok, S. M. Cotin, M. P. Ottensmeyer, A. M. Galea, R. D. Howe and S. L. Dawson, "Truth cube: establishing physical standards for soft tissue simulation," Med. Image Anal. 7(3), 283-291 (2003).

[11]S. P. DiMaio, S. E. Salcudean, "Needle insertion modeling and simulation," *Proceedings of the IEEE International Conference on Robotics and Automation – ICRA*, (Washington, DC, 2002), pp. 2098-2105.

[12]J. R. Crouch, C. M. Schneider, J. Wainer and A. M. Okamura, "A Velocity-Dependent Model for Needle Insertion in Soft Tissue," *Med. Image Comput. Comput. Assist. Interv. – MICCAI*, 8 (Pt 2), 624-632 (2005).

[13]J. Bax, D. Cool, L. Gardi, K. Knight, D. Smith, J. Montreuil, S. Sherebrin, C. Romagnoli and A. Fenster, "Mechanically assisted 3D ultrasound guided prostate biopsy system," Med. Phys. 35(12), 5397-5410 (2008).

[14]J. A. Long, V. Daanen, A. Moreau-Gaudry, J. Troccaz, J. J. Rambeaud and J. L. Descotes, "Prostate biopsies guided by 3-dimension real-time (4D) transrectal ultrasound on a phantom. Comparative study versus 2D transrectal ultrasound guided biopsies," Prog. Urol. 17(7), 1337-1342 (2007).

[15]X. Wen and S. E. Salcudean, "Detection of Brachytherapy Seeds Using 3D Transrectal Ultrasound," *Proceedings of the Annual International Conference of the IEEE Engineering in Medicine and Biology Society*, (Vancouver, BC, 2008), pp. 855-858.

[16]J. A. Cunha, I. C. Hsu, J. Pouliot, I. M. Roach, K. Shinohara, J. Kurhanewicz, G. Reed and D. Stoianovici, "Toward adaptive stereotactic robotic brachytherapy for prostate cancer: Demonstration of an adaptive workflow incorporating inverse planning and an MR stealth robot," Minim. Invasive Ther. Allied Technol. 19(4), 189-202 (2010).

[17]J. P. McGahan, J. Ryu and M. Fogata, "Ultrasound probe pressure as a source of error in prostate localization for external beam radiotherapy," Int. J. Radiat. Oncol. Biol. Phys. 60(3), 788-93 (2004).

[18]E. Dehghan, X. Wen, R. Zahiri-Azar, M. Marchal, S. E. Salcudean, "Needle-tissue interaction modeling using ultrasound-based motion estimation: Phantom study," Comput. Aided. Surg. 13(5), 265-280 (2008).

[19]J. Sherman J, T. K. Podder, V. Misic, L. Fu, D. Fuller, B. Winey, E. M. Messing, D. J. Rubens, J. G. Strang, R. Brasacchio and Y. Yu, "Efficacy of Prostate Stabilizing Techniques during Brachytherapy Procedure." *Proceedings of the Annual International Conference of the IEEE Engineering in Medicine and Biology Society*, (New York, NY, 2006) pp. 563-566.

[20]J. E. Browne, K. V. Ramnarine, A. J. Watson and P. R. Hoskins, "Assessment of the acoustic properties of common tissue-mimicking test phantoms," Ultrasound Med. Biol. 29(7), 1053-1060 (2003).

[21]K. Zell, J. I. Sperl, M. W. Vogel, R. Niessner and C. Haisch, "Acoustical properties of selected tissue phantom materials for ultrasound imaging," Phys. Med. Biol. 52(20), N475-484 (2007).

[22]T. J. Hall, M. Bilgen, M. F. Insana and T. A. Krouskop, "Phantom Materials for Elastography," IEEE Trans. Ultrason Ferroelectr Freq Control, 44(6), 1355 – 1365 (1997).

[23]K. J. Surry, H. J. Austin, A. Fenster and T. M. Peters, "Poly(vinyl alcohol) cryogel phantoms for use in ultrasound and MR imaging," Phys. Med. Biol. 49(24), 5529-5546 (2004).

[24]J. Fromageau, J. L. Gennisson, C. Schmitt, R. L. Maurice, R. Mongrain and G. Cloutier, "Estimation of polyvinyl alcohol cryogel mechanical properties with four ultrasound elastography methods and comparison with gold standard testings," IEEE Trans. Ultrason. Ferroelectr. Freq. Control, 54(3), 498-509 (2007).

[25]C. U. Devi, R. M. Vasu, A. K. Sood, "Design, fabrication, and characterization of a tissue-equivalent phantom for optical elastography," J. Biomed. Opt. 10(4),44020 (2005).

[26]G. M. Spirou, A. A. Oraevsky, I. A. Vitkin and W. M. Whelan, "Optical and acoustic properties at 1064 nm of polyvinyl chloride-plastisol for use as a tissue phantom in biomedical optoacoustics," Phys. Med. Biol. 50(14), N141-N153 (2005).

[27]E. L. Madsen, G. R. Frank, T. A. Krouskop, T. Varghese, F. Kallel and J. Ophir, "Tissue-Mimicking Oil-in-Gelatin Dispersions for Use in Heterogeneous Elastography Phantoms," Ultrason. Imaging, 25(1), 17-38 (2003).

[28]M. B. Zerhouni and M. Rachedine, "Ultrasonic calibration material and method," US Patent 5196343 (1993).

[29]M. M. Doyley, J. C. Bamber, F. Fuechsel and N. L. Bush, "A freehand elastographic imaging approach for clinical breast imaging: system development and performance evaluation," Ultrasound Med. Biol. 27(10), 1347-1357 (2001).

[30]W. D. D'Souza, E. L. Madsen, O. Unal, K. K. Vigen, G. R. Frank and B. R. Thomadsen, "Tissue mimicking materials for a multi-imaging modality prostate phantom," Med. Phys. 28(4), 688-700 (2001).

[31]E. L. Madsen, M. A. Hobson, H. Shi, T. Varghese, and G. R. Frank, "Tissue-mimicking agar/gelatin materials for use in heterogeneous elastography phantoms," Phys. Med. Biol. 50(23), 5597-55618 (2005).

[32]B. W, Pogue and M. S. Patterson, "Review of tissue simulating phantoms for optical spectroscopy, imaging and dosimetry," J. Biomed. Opt. 11(4), 1-16 (2006).

[33]Z. Bu-Lin, J. Bing, K. Sheng-Li, Y. Huang, W. Rong and L. Jia, "A polyacrylamide gel phantom for radiofrequency ablation," Int. J. Hyperthermia, 24(7), 568-576 (2008).

[34]U. Lindner, N. Lawrentschuk, R. A. Weersink, O. Raz, E. Hlasny, M. S. Sussman, S. R. Davidson, M. R. Gertner and J. Trachtenberg, "Construction and evaluation of an anatomically correct multi-image modality compatible phantom for prostate cancer focal ablation," J. Urol. 184(1), 352-357 (2010).

[35]M. McDonald, S. Lochhead, R. Chopra and M. J. Bronskill, "Multi-modality tissue-mimicking phantom for thermal therapy," Phys. Med. Biol. 49(13), 2767-2778 (2004).

[36]H. Kato, M. Kuroda, K. Yoshimura, A. Yoshida, K. Hanamoto, S. Kawasaki, K. Shibuya and S. Kanazawa, "Composition of MRI phantom equivalent to human tissues," Med. Phys. 32(10), 3199-3208 (2005).

[37]T. Kondo, M. Kitatuji and H. Kanda, "New Tissue Mimicking Materials for Ultrasound Phantoms," *IEEE Ultrasonics Symposium*, (Rotterdam, The Netherlands, 2005) pp. 1664 – 1667.

[38]T. Podder, D. Clark, J. Sherman, D. Fuller, E. Messing, D. Rubens, J. Strang, R. Brasacchio, L. Liao, W. S. Ng and Y.Yu, "In vivo motion and force measurement of surgical needle intervention during prostate brachytherapy," Med. Phys. 33(8), 2915-2922 (2006).

[39]D. Fontanarosa, S. van der Meer, E. Harris and F. Verhaegen, "A CT based correction method for speed of sound aberration for ultrasound based image guided radiotherapy," Med. Phys. 38(5), 2665-2673 (2011).

[40]D. Pfeiffer, S. Sutlief, W. Feng, H. M. Pierce and J. Kofler, "AAPM Task Group 128: Quality assurance tests for prostate brachytherapy ultrasound systems," Med. Phys. 35, 5471-5489 (2008).

[41]E. J. Chen, J. Novakofski, W. K. Jenkins and W. D. O'Brien, "Young's Modulus Measurements of Soft Tissues with Application to Elasticity Imaging," IEEE Trans. Ultrason. Ferroelectr. Freq. Control, 43(1), 271-275 (1996).

[42]K. J. Parker, S. R. Huang, R. M. Lerner, F. Lee, D. Rubens, and, Roach, "Elastic and ultrasonic properties of the prostate," *IEEE Ultrasonics Symposium*, (1993) 1035-1038.

[43]T. A. Krouskop, T. M. Wheeler, F. Kallel, B. S. Garra and T. Hall, "Elastic moduli of breast and prostate tissues under compression," Ultrason. Imaging. 20(4), 260-274 (1998).

[44]K. S. Arun, T. S. Huang and S. D. Blostein, "Least-Squares Fitting of Two 3-D Point Sets," IEEE Trans. Pattern Analysis and Machine Intelligence, PAMI-9(5), 698-700 (1987).

[45]B. Maurin, L. Barbé, B. Bayle, P. Zanne, J. Gangloff, M. de Mathelin, A. Gangi, L. Soler and A. Forgione, "In Vivo Study of Forces During Needle Insertions. Proceedings of the Medical Robotics," *Navigation and Visualisation Scientific Workshop* (Remagen, Germany, 2004).

[46]H. Kataoka, T. Washio, K. Chinzei, K. Mizuhara, C. Simone and A. M. Okamura, "Measurement of the Tip and Friction Force Acting on a Needle during Penetration," *Med. Image Comput. Comput. Assist. Interv. – MICCAI*, 2002, (2002) pp. 216–223.

[47]R. Taschereau, J. Pouliot, J. Roy and D. Tremblay, "Seed misplacement and stabilizing needles in transperineal permanent prostate implants," Radiother. Oncol. 55(1), 59-63 (2000).

[48]N. N. Stone, J. Roy, S. Hong, Y. C. Lo and R. G. Stock, "Prostate gland motion and deformation caused by needle placement during brachytherapy," Brachytherapy, 1(3), 154-160 (2002).

[49]V. Lagerburg, M. A. Moerland, J. J. Lagendijk, J. J. Battermann, "Measurement of prostate rotation during insertion of needles for brachytherapy," Radiother. Oncol. 77(3), 318-323 (2005).

## TABLES & FIGURE CAPTIONS:

TABLE I. Properties, found in the literature, of the typical soft materials used in phantom construction. All values were reported at room temperature.

| Material | Density (kg/m$^3$) | Young's Modulus (kPa) | Speed of Sound (m/s) | Attenuation (dB/cm/MHz) | Measurement Frequency (MHz) | T1 Relax. Time (ms) | T2 Relax. Time (ms) | Ref. |
|---|---|---|---|---|---|---|---|---|
| Agarose | 1036 ± 22 | | | | | 1207 ± 168 | 66 ± 9 | 9 |
| Agarose | | | 1546 | 0.5 | 2.0-10.0 | | | 20 |
| Agarose | 1040 ± 11 | | 1050 ± 30 | 0.08 ± 0.02 | 5 | | | 21 |
| Agar | | 7.6-195 | | | | | | 22 |
| PVA-C | | | 1520-1540 | 0.075-0.22 | 3.0-8.0 | 718-1034 | 108-175 | 23 |
| PVA-C | 1028-1054 | 0.2-6 | 1525-1560 | | | | | 24 |
| PVA-C | 1100 ± 50 | | 1570 ± 20 | 0.58 ± 0.02 | 5 | | | 21 |
| PVA-C | 1015-1027 | | 1524.4-1570.5 | 1.4-2.9 | 2.2 | | | 25 |
| PVC | 1000 ± 40 | | 1400 ± 20 | 0.56 ± 1.01 | 0.61-1.25 | | | 26 |
| PVC | | | 1395 | 1.05-1.37 | 4.5-8.0 | | | 27 |
| PVC | | 10-100 | | | | | | 11 |
| Silicone | 1070 ± 30 | | 1030 ± 60 | 2.8 ± 0.28 | 5 | | | 21 |
| Silicone | | 0.2-2 | | | | | | 8 |
| Silicone | | 25.8 | | | | | | 10 |
| Zerdine | | | 1420-1650 | 0.1-1.5 | 2.0-10.0 | | | 28 |
| Zerdine | | | 1538 | 0.7 | 4 | | | 20 |
| Gelatin | | 4.8-158 | 1555-1598 | | | | | 22 |
| Gelatin | | 104 ± 3 | 1538 | 0.1-0.19 | 2.5-8.0 | 1610 | 416 | 27 |

TABLE II. Ratios of hardener to softener used to make the various PVC mixtures used in our phantom. ρ is density, c is speed of sound, E is elastic modulus and H is Hounsfield.

| Mixture name | Hardener | Softener | ρ (kg/m$^3$) | c (m/s) | E (kPa) | H. Unit |
|---|---|---|---|---|---|---|
| Super rigid (hardener) | 100% | 0% | - | - | 200 | - |
| Rigid | 75% | 25% | 0.98 | 1580 | 150 | 100-110 |
| Standard | 50% | 50% | 0.91 | 1440 | 100 | 60-80 |
| Soft | 25% | 75% | 0.93 | 1420 | 50 | 30-50 |
| Super soft | 10% | 90% | 0.74 | 1360 | 3 | -20-15 |

TABLE III. Results showing the translation and rotation of the prostate during needle insertion into the phantom.

| Insertion # | Translation (mm) | Rotation (deg.) | | |
|---|---|---|---|---|
| | | Coronal | Sagittal | Transverse |
| 1 | 3.7 | 0.3 | -0.2 | 0 |
| 2 | 2.3 | 1.0 | 0.3 | 0.9 |
| 3 | 2.4 | -1.2 | -0.4 | -1.3 |
| 4 | 2.7 | 0 | -2.1 | -0.1 |
| 5 | 3.3 | 0.3 | 1.1 | 0 |

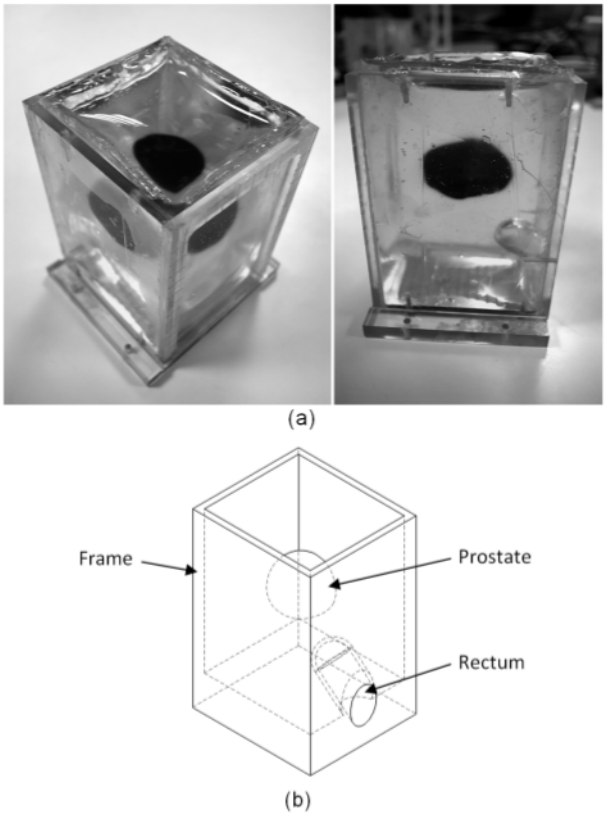


FIG. 1. (a) Photograph of the phantom with mobile prostate and rectum. (b) CAD drawing of phantom. Note that the rectum shown in this figure is meant for an end-fire US probe. For side-fire probes, a cylindrical rectum is used, as shown in Figure 11.

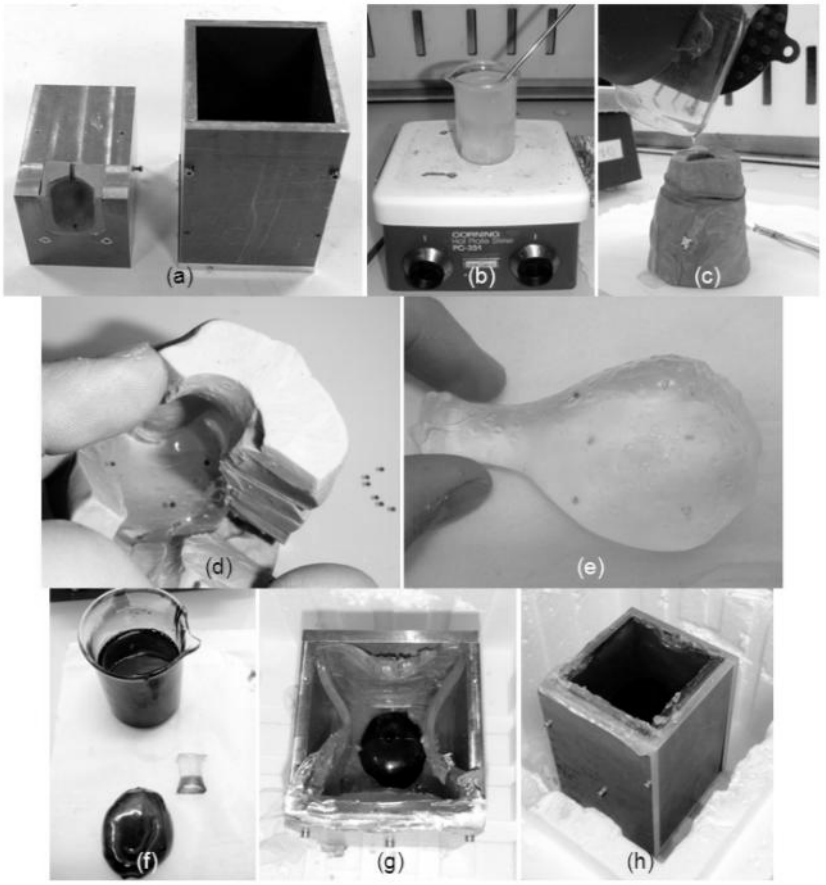


FIG. 2. Steps during construction of the prostate phantom. (a) Mould used to shape the outer frame of the phantom. (b) Heating of the PVC mixture. (c) Pouring the molten PVC into the prostate mould. (d) Placing the targets onto the first layer of the prostate. (e) The final prostate shape. (f) Coating the prostate with an echogenic stained PVC mixture. (g) Putting the prostate in place inside the frame. (h) Allowing the phantom to cool overnight.

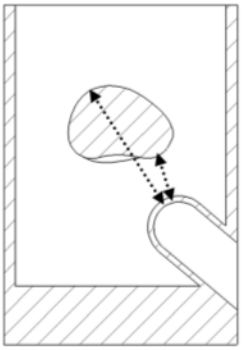

FIG. 3. The shallowest and deepest trajectories from the probe head, used to calculate the range of sound speeds in the phantom.

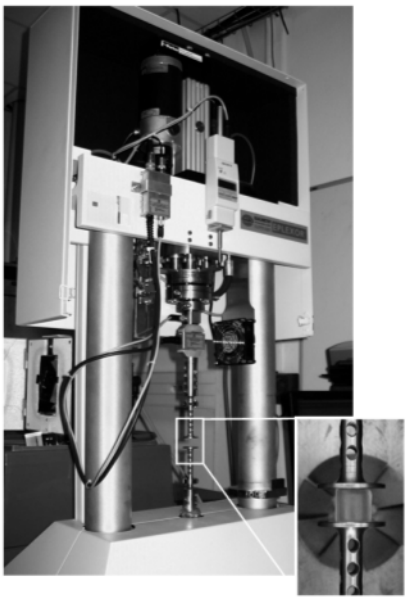

FIG. 4. Mechanical characterization machine used to measure the compression stress-strain relationship of the PVC samples. The inlayed image shows a sample in place between the compression rods.

530

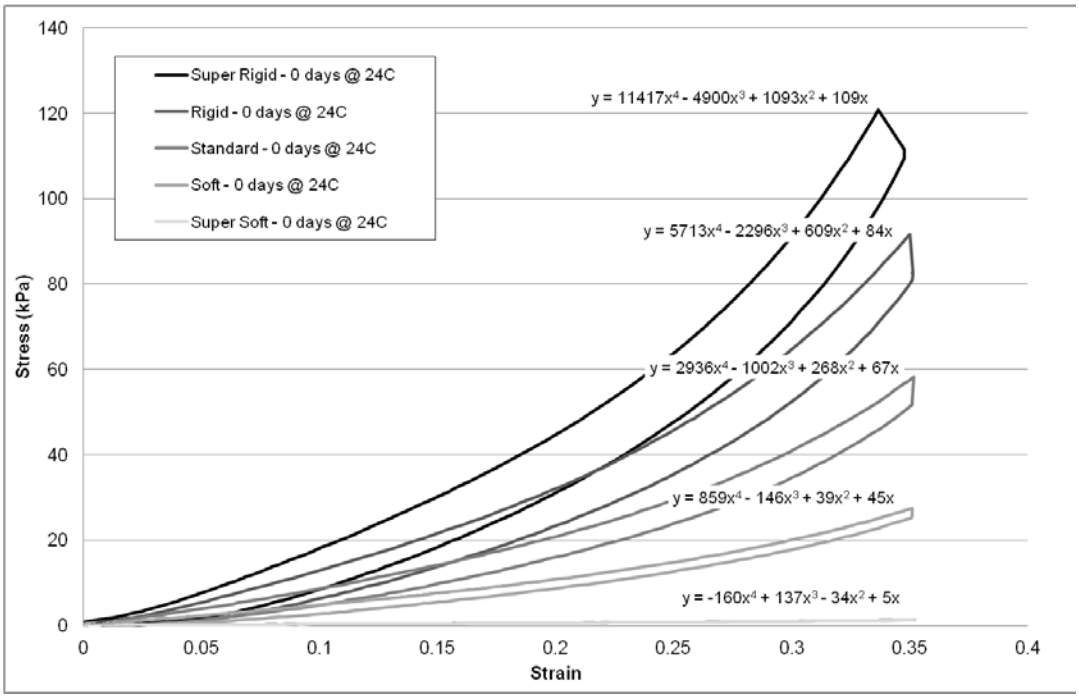


FIG. 5. Stress-strain curves for the five sets of PVC samples. The displayed equations represent the polynomial fits for the compression phase (upper part) of each curve.

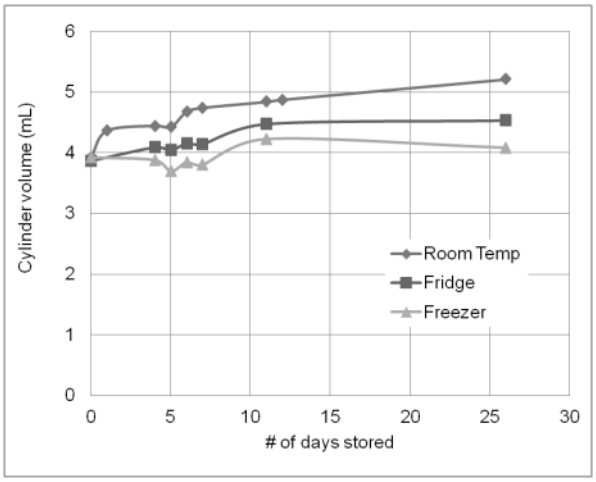


FIG. 6. Volume over time of the thresholded inclusions for the three samples stored at different temperatures. The uneven jumps in the curves are likely the result of slight image inconsistencies caused by variable probe pressure or the presence of air bubbles in ultrasound gel applied at the probe-phantom interface.

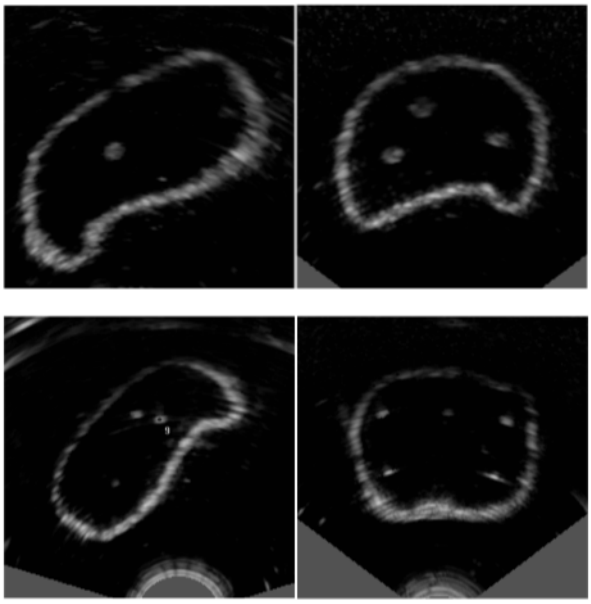

FIG. 7. Sagittal (left images) and transverse (right images) cuts of 3D ultrasound volumes taken of two different phantoms. The top images are of a phantom with 3mm polymer clay targets embedded in the prostate, while bottom images show a phantom embedded with 1mm glass targets. Note that the oblique angle of the prostate in the sagittal images is due to the use of an obliquely-placed end-fire probe.

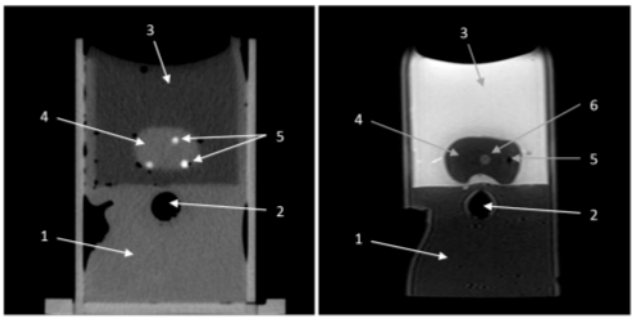


FIG. 8. Transverse cuts of a CT (left) and an MR (right) volume of two different phantoms. The left phantom has polymer clay embedded targets. The right phantom has a urethra. 1: Frame, 2: rectum, 3: periprostatic material, 4: prostate, 5: polymer clay targets, 6: urethra.

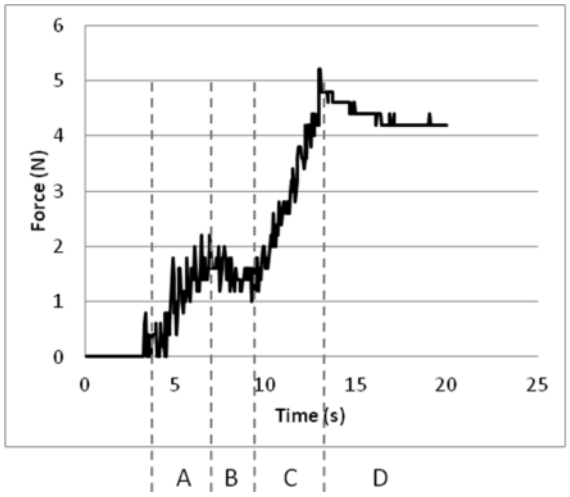


FIG. 9. Axial needle force measured during needle insertion into our phantom. A denotes the needle traversing the perineum. B denotes the super soft PVC before reaching the prostate. C denotes the prostate. D denotes the relaxation of the material after stopping needle motion.

535

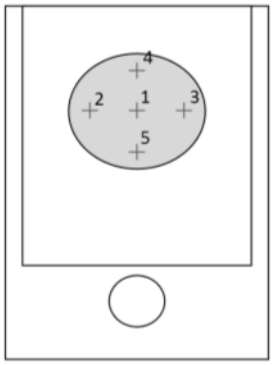


FIG. 10. Needle insertion locations used for phantom deformation testing.


FIG. 11. Prostate phantom with a horizontal cylindrical rectum, being used with a side-fire US probe during a mock brachytherapy test.